Journal of Saudi Chemical Society (2023) **27**, 101598

King Saud University

Journal of Saudi Chemical Society

www.ksu.edu.sa
www.sciencedirect.com

Synthesis, pharmacological evaluation, and molecular modeling studies of novel isatin hybrids as potential anticancer agents

Rajapandi Raju [a,*], Kumarappan Chidambaram [b,*], Balakumar Chandrasekaran [c], Mohammad F. Bayan [c], Tapan Kumar Maity [d], Abdullah M. Alkahtani [e], Harish C Chandramoorthy [e,f]

[a] *Department of Pharmaceutical Chemistry, Arulmigu Kalasalingam College of Pharmacy, Krishnankovil- 626126, Tamilnadu, India*
[b] *Department of Pharmacology, College of Pharmacy, King Khalid University, P. O. Box: 960, Abha 61421, Saudi Arabia*
[c] *Faculty of Pharmacy, Philadelphia University, P.O. Box 1, Amman, 19392, Jordan*
[d] *Department of Pharmaceutical Technology, Division of Pharmaceutical Chemistry, Jadavpur University, Kolkata 700032, India*
[e] *Department of Microbiology & Clinical Parasitology, College of Medicine, King Khalid, University, Al-Qara, Saudi Arabia*
[f] *Center for Stem Cell Research, College of Medicine, King Khalid University, Al-Qara, Saudi Arabia*

Received 13 March 2022; revised 24 December 2022; accepted 31 December 2022
Available online 5 January 2023

KEYWORDS

Isatin-pyrimidine hybrid;
Antiproliferative activity;
Breast cancer cell (MCF-7);
Dalton's ascitic lymphoma (DAL);
Molecular docking

Abstract A novel series of isatin hybrids **5a-g** was designed, synthesized, and characterized spectroscopically. The synthesized compounds were evaluated for their cytotoxic activity against the human breast cancer cell line (MCF-7) by *in vitro* MTT assay. Amongst the tested compounds, **5e** compound bearing benzyl moiety at N_4 piperazine was found to be the most active with the promising IC_{50} (12.47 μM). Moreover, the active compounds **5e** and **5g** were subjected to antitumor evaluation (*in vivo*) against Dalton's ascitic lymphoma (DAL) cell line and the results suggested that the best active compound **5e** can normalize the blood picture in comparison to the standard drug. An *in silico* molecular docking study using the crystal structure of Hsp90 protein described the role

Abbreviations ADME, absorption distribution metabolism and excretion; ANOVA, analysis of variance; DAC, dalton's ascitic lymphoma; DHFR, dihydrofolate reductase; DMF, dimethylformamide; DMSO, dimethylsulfoxide; DNA, deoxyribonucleic acid; ESI, MS, electrospray ionization mass spectrometry; 5, FU, fluorouracil; FT, IR, fourier transform infrared spectroscopy; HIA, Human intestinal absorption; Hsp90, heat shock protein 90; IC_{50}, the concentration of drug required for 50% inhibition; ILS, increase in life span; KBr, potassium bromide; LD_{50}, the median lethal dose; MCF, 7, human breast cancer cell line; MST, median survival time; MTT, 3, (4,5, dimethylthiazol, 2, yl), 2,5, diphenyltetrazolium bromide; NMR, nuclear magnetic resonance; PDB, protein data bank; RBC, red blood cells; RNA, ribonucleic acid; SAR, structure, activity relationship; SEM, standard error of the mean; TLC, thin, layer chromatography; TMS, tetramethylsilane; WBC, white blood cells

* Corresponding authors.
E-mail addresses: rajarishi05@gmail.com (R. Raju), kumarappan@kku.edu.sa (K. Chidambaram).

Peer review under responsibility of King Saud University. Production and hosting by Elsevier.

Production and hosting by Elsevier

https://doi.org/10.1016/j.jscs.2023.101598

of significant protein–ligand interactions and revealed more insights into the binding mode. The drug-likeliness of the compounds was predicted based on Lipinski's rule of five and pharmacokinetic ADME parameters. Hence, the synthesized isatin hybrids could be novel starting point anticancer lead compounds demonstrating drug-like properties which can be explored further for anticancer drug discovery.

1. Introduction

Cancer is the second leading cause of death and is alone responsible for 10 million deaths reported worldwide in the year 2020. Twenty-two million new cancer cases will be anticipated by the year 2030. Approximately, 70 % of cancer deaths are recorded in low- and middle-income countries. Breast cancer is the major cause of death among the female population, accounting for half a million per year [1]. The social and economic burdens associated with cancers are severe at national and international levels. In general, chemotherapy includes the administration of chemical-based drugs to arrest the growth or survival of cancer cells. The current chemotherapy is less effective to combat cancer due to multiple reasons such as genetic variation, mutation of genes, inability to target specific proteins, and altered lifestyle. Though there have been developments in the diagnosis, prevention, and treatment of cancer; a successful therapy to treat cancer remains challenging to date. However, most of the chemotherapeutic agents are non-specific and destroy the host cells. Moreover, mutations and drug resistance are adding more problems during the treatment of cancers with chemotherapeutic drugs [2]. Thus, there is an urgent need to develop new, safe and efficacious anti-cancer therapeutics or agents exhibiting a broad spectrum of activity without host cell toxicity.

It is well documented in the literature that isatin (1*H*-indole-2,3-dione) is one of the versatile building blocks in medicinal compounds due to the wide range of pharmacological activities including antiviral [3], antiangiogenic [4], anticancer [5], antimalarial [6], antimicrobials [7]. On the other hand, pyrimidine is also an active core structure present in a large variety of pharmaceutical compounds. Due to the presence of pyrimidine moiety in thymine, cytosine, and uracil which are considered as pyrimidine-bases of nucleic acids (DNA and RNA). The differently substituted pyrimidine derivatives showed antitumor activity against different human carcinoma cell lines [8,9]. Similarly, 2,4-diamino-5-benzylpyrimidine exhibited significant antimicrobial and antifolate activity by inhibiting non-classical dihydrofolate reductase (DHFR) [10].

In the design of new bioactive medicinal agents, the concept of hybridization through the combination of different pharmacophores in the same molecular architecture yields medicinally active compounds exhibiting synergistic biological activities [11,12]. Moreover, few hybrid compounds of isatin are reported in the literature for their varied biological applications [13–17]. Some of the literature reported biologically active novel isatin and pyrimidine hybrids leading to the design of the target compound is depicted in Fig. 1.

These inspiring investigations and in continuation of our medicinal chemistry research, we envisaged to design, synthesize and evaluate novel isatin-pyrimidine hybrids as potential anticancer agents against human breast cancer cell line (MCF-7) by *in vitro*. Further, we determined *in vivo* antitumor activity against the mice model of Dalton's ascitic lymphoma (DAL). To better gain an understanding of the possible molecular target and the binding mode of the synthesized compounds, an *in silico* molecular docking study was performed using the molecular structure Hsp90 protein. Further, *in silico* drug-like properties and pharmacokinetic ADME properties were also computed to establish the drug-likeliness of the synthesized compounds.

2. Materials and methods

2.1. General

All the reagents, solvents, and chemicals were obtained from Aldrich Chemicals Company (USA) or Merck and were used as received without further purification unless otherwise stated. The progress of the reactions and the purity of the compounds was monitored by thin-layer chromatography (TLC) on precoated silica gel plates procured from E. Merck and Co. (Darmstadt, Germany) visualized by UV lamp (254 or 365 nm). Melting points were recorded on a SPAC-A Service (India) open capillary melting point apparatus (Laboratory device) and are uncorrected. Infrared spectra were recorded using JASCO FT-IR Model-410 by KBr discs method and spectra were calibrated against the polystyrene absorption at 1601 cm^{-1}. The NMR spectra were recorded on a Bruker DPX 300 MHz NMR instrument at ambient temperature using DMSO d_6 as a solvent. Chemical shift values are reported in parts per million under δ scale in relative to the internal standard tetramethylsilane (TMS). Mass spectrometry (ESI-MS) data are given in the *m*/*z* unit. Elemental analysis was determined on a Perkin Elmer 2400 CHN Elemental Analyzer.

2.2. Synthesis of 3-{[4-amino-5-(furan-2-ylmethyl) pyrimidin-2-yl] imino}-1, 3-dihydro-2H-indol-2-one (3)

Equimolar quantities of 5-(furan-2-ylmethyl) pyrimidine-2,4-diamine (**1,** 0.01 mol) and isatin (**2,** 0.01 mol) were dissolved in warm ethanol containing 1 ml of glacial acetic acid and the mixture was heated under reflux on a water bath for 24 h. The precipitated product was collected and recrystallized using ethanol. Yield: 76.5 %; m.p.: 220℃. IR (KBr, cm^{-1}): 3449 (N—H str. of NH_2), 3314 (N—H str. of NH_2), 3139 (C—H str.), 2882, 2745, 1617 (C=N str.), 1485, 1266, 1140, 892, 740, 765; ^{1}H NMR (300 MHz, DMSO d_6) δ: 3.65 (s, 2H, C$\underline{H}_2$ of furfuryl), 5.70 (s, 2H, N$\underline{H}_2$), 6.60 (m, 1H, Furan-H), 6.87–6.93 (m, 2H, Ar-H and furan-H), 7.05–7.10

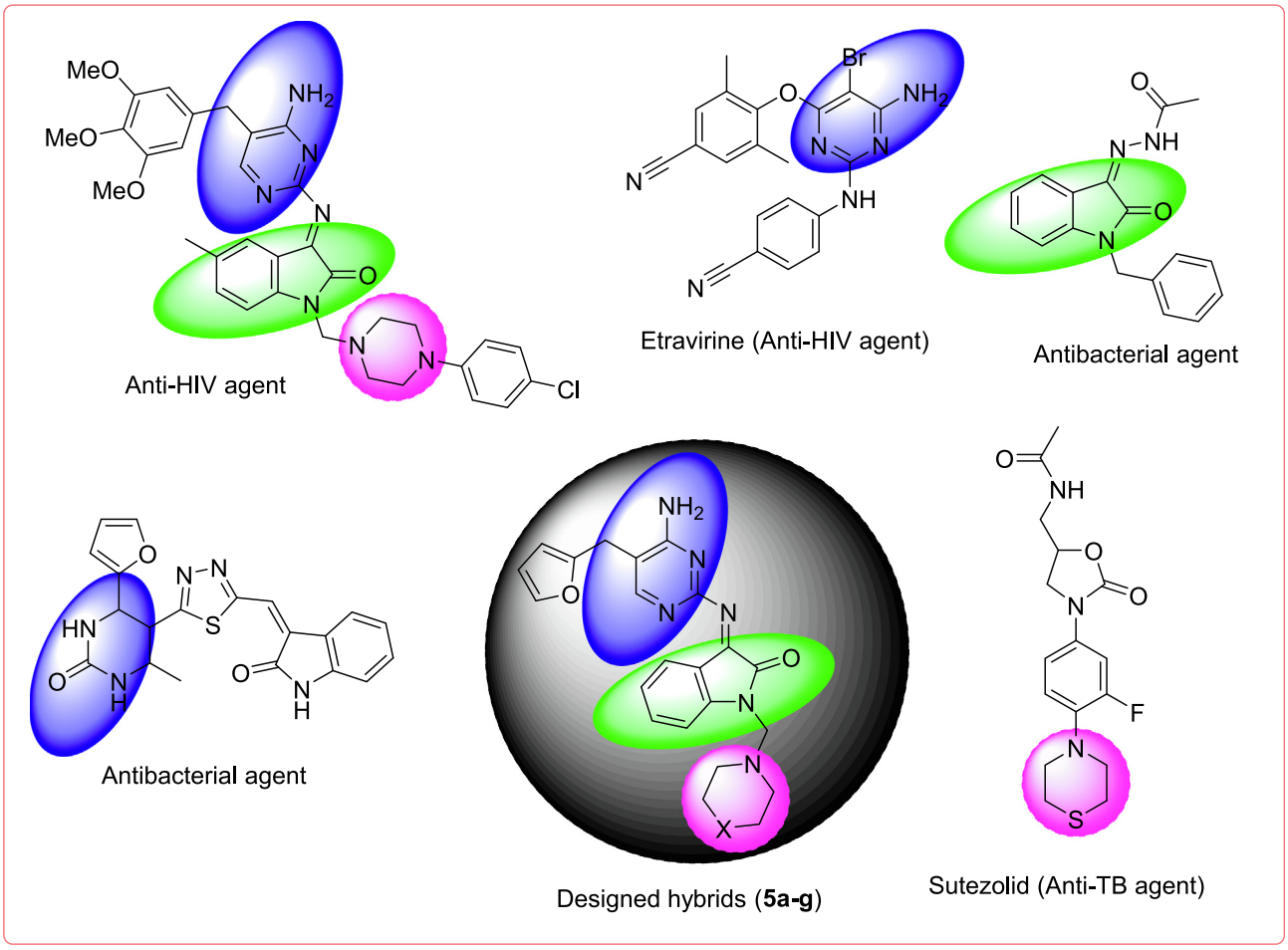

Fig. 1 Some of the reported biologically active isatin and pyrimidine scaffolds to design **5a-g**.

(m, 2H, Ar-H), 7.49–7.52 (m, 2H, Ar-H and furan-H), 7.79 (m, 1H, Ar-H), 11.07 (s, 1H, NH) ppm; ESIMS *m/z*: 320 $[M + H]^+$. Elemental analysis: Anal. calcd. for: $C_{17}H_{13}N_5O_2$: C, 63.94; H, 4.10; N, 21.93; O, 10.02. Found: C, 63.94; H, 4.14; N, 21.92; O, 10.13.

2.3. General procedure for the synthesis of isatin-pyrimidine hybrids (5a-g)

Equimolar quantities of intermediate compound **3** (0.01 mol) and the heterocyclic secondary amines **4a-g** (0.01 mol) were taken in glacial acetic acid (25 ml) and added 37 % formaldehyde solution (1 ml). The reaction mixture was heated under reflux over the water bath for 1–3 hr. Upon completion of the reaction as monitored by TLC, the reaction mixture was concentrated to approximately half of the initial volume. Thus, the resulting precipitate was isolated by filtration and recrystallized using a mixture of DMF and water to afford pure final compounds **5a-g.**

2.3.1. 3-(4-Amino-5-furan-2-ylmethyl-pyrimidin-2-ylimino)-1-piperazine-1-ylmethyl-1,3-dihydro-indol-2-one (5a)

Yellow crystals; yield: 65 %; m.p.: 285 – 287℃. IR (KBr, cm^{-1}): 3440, 3100, 2880, 2745, 2230, 1600, 1485, 1266, 1147, 892, 765, 720; ^{1}H NMR (300 MHz, DMSO d_6) δ: 2.04–2.09 (m, 8H piperazine-H), 2.24 (s, 1H, NH), 3.65 (s, 2H, C<u>H</u>$_2$ of furfuryl), 4.39 (s, 2H, N-C<u>H</u>$_2$-N), 5.70 (s, 2H, NH_2), 6.90–7.15 (m, 3H, Furan-H), 7.23–7.65 (m, 4H, Ar-H) ppm, 8.23 (m, 1H, Ar-H); ESI-MS *m/z*: 418 $[M + H]^+$. Elemental analysis: Anal. calcd. for: $C_{22}H_{23}N_7O_2$: C, 63.30; H, 5.55; N, 23.49; O, 7.66. Found: C, 63.24; H, 5.50; N, 23.48; O, 7.61.

2.3.2. 3-(4-Amino-5-furan-2-ylmethyl-pyrimidin-2-ylimino)-1-(4-methyl-piperazine-1-ylmethyl-1, 3-dihydro-indol-2-one (5b)

Yellow crystals; yield: 70 %; m.p.: 205 – 209℃. IR (KBr, cm^{-1}): 3450, 3120, 2882, 2727, 2200, 1645, 1485, 1266, 1147, 985, 920, 892, 760, 740; ^{1}H NMR (300 MHz, DMSO d_6): 2.04 (s, 3H, C<u>H</u>$_3$ of piperazine), 2.17–2.19 (m, 8H, piperazine H), 3.48 (s, 2H, CH_2 of furfuryl), 4.39 (s, 2H, N-C<u>H</u>$_2$-N), 6.17 (s, 2H, NH_2), 6.90–7.09 (m, 3H, Furan-H), 7.23–7.83 (m, 5H, Ar-H) ppm; ESI-MS *m/z*: 432 $[M + H]^+$. Elemental analysis: Anal. calcd. for: $C_{23}H_{25}N_7O_2$: C, 64.02; H, 5.84; N, 22.72; O, 7.42. Found: C, 64.11; H, 5.81; N, 22.68; O, 7.39.

2.3.3. 3-(4-Amino-5-furan-2-ylmethyl-pyrimidin-2-ylimino)-1-(4-ethyl-piperazine-1-ylmethyl-1, 3-dihydro-indol-2-one (5c)

Yellow crystals; yield: 58 %; m.p.: 215 – 217℃. IR (KBr, cm^{-1}): 3454, 3100, 2882, 2737, 2230, 1628, 1485, 1266, 1147, 892, 855, 775, 745, 710; ^{1}H NMR (300 MHz, DMSO d_6) δ: 1.54 (t, 3H, C<u>H</u>$_3$ of C_2H_5), 2.04–2.19 (m, 8H, piperazine H), 3.48 (s, 2H, CH_2 of furfuryl), 3.9 (q, 2H, C<u>H</u>$_2$ of C_2H_5), 4.39

(s, 2H, N-C<u>H</u>$_2$-N), 6.17 (s, 2H, NH_2), 6.90–7.09 (m, 3H, Furan-H), 7.23–7.83 (m, 5H, Ar-H) ppm; ESI-MS *m/z*: 446 $[M + H]^+$. Elemental analysis: Anal. calcd. for: $C_{24}H_{27}N_7O_2$: C, 64.70; H, 6.11; N, 22.01; O, 7.18. Found: C, 64.70; H, 6.10; N, 22.04; O, 7.13.

2.3.4. 3-(4-Amino-5-furan-2-ylmethyl-pyrimidin-2-ylimino)-1-(4-phenyl-piperazine-1-ylmethyl-1, 3-dihydro-indol-2-one (5d)

Yellow crystals; yield: 80 %; m.p.:180 − 185℃. IR (KBr, cm^{-1}): 3440, 3145, 2882, 2737, 2230, 1628, 1400, 1266, 1147, 892, 820, 745, 720; ^{1}H NMR (300 MHz, DMSO d_6) δ: 2.0–2.12 (m, 8H, piperazine H), 3.41 (s, 2H, C<u>H</u>$_2$ of furfuryl), 4.74 (s, 2H, N-C<u>H</u>$_2$-N), 4.91 (s, 2H, NH_2), 6.17–6.92 (m, 3H, Furan-H), 7.04–8.14 (m, 10*H*, Ar-H) ppm; ESI-MS *m/z*: 494 $[M + H]^+$. Elemental analysis: Anal. calcd. for: $C_{28}H_{27}N_7O_2$: C, 68.14; H, 5.51; N, 19.87; O, 6.48. Found: C, 68.18; H, 5.52; N, 19.86; O, 6.48.

2.3.5. 3-(4-Amino-5-furan-2-ylmethyl-pyrimidin-2-ylimino)-1-(4-benzyl- piperazine-1-ylmethyl)-1, 3-dihydro-indol-2-one (5e)

Yellow crystals; yield: 45 %; m.p. > 300℃. IR (KBr, cm^{-1}): 3409, 3119, 2882, 2737, 2230, 1628, 1485, 1266, 1147, 892, 835, 745, 710; ^{1}H NMR (300 MHz, DMSO d_6) δ: 2.01–2.14 (m, 8H, piperazine H), 3.38 (s, 2H, C<u>H</u>$_2$ of furfuryl), 3.70, (s, 2H, C<u>H</u>$_2$ of benzyl), 4.70 (s, 2H, N-C<u>H</u>$_2$-N), 4.92 (s, 2H, NH_2), 6.19–6.89 (m, 3H, Furan-H), 7.14–8.19 (m, 10*H*, Ar-H) ppm; ESI-MS *m/z*: 508 $[M + H]^+$. Elemental analysis: Anal. calcd. for: $C_{29}H_{29}N_7O_2$: C, 68.62; H, 5.76; N, 19.32; O, 6.30. Found: C, 68.62; H, 5.72; N, 19.31; O, 6.28.

2.3.6. 3-(4-Amino-5-furan-2-ylmethyl-pyrimidin-2-ylimino)-1-morpholin-4- ylmethyl-1, 3-dihydro-indol-2-one (5f)

Pale yellow crystals; yield: 55 %; m.p.:155 − 160℃. IR (KBr, cm^{-1}): 3490, 3009, 2882, 2737, 2230, 1628, 1485, 1266, 1147, 892, 810, 745, 710; ^{1}H NMR (300 MHz, DMSO d_6) δ: 2.09–2.49 (m, 8H, morpholino-H), 3.31 (s, 2H, C<u>H</u>$_2$ of furfuryl), 3.54 (s, 2H, N-C<u>H</u>$_2$-N), 4.38 (s, 2H, NH_2), 6.91–7.16 (m, 3H, Furan-H), 7.26–7.68 (m, 4H, Ar-H), 8.14 (m, 1H, Ar-H) ppm; ESI-MS *m/z*: 419 $[M + H]^+$. Elemental analysis: Anal. calcd. for: $C_{22}H_{22}N_6O_3$: C, 63.15; H, 5.30; N, 20.08; O, 11.47. Found: C, 63.14; H, 5.34; N, 20.08; O, 11.44.

2.3.7. 3-(4-Amino-5-furan-2-ylmethyl-pyrimidin-2-ylimino)-1-piperidin-1- ylmethyl-1, 3-dihydro-indol-2-one (5g)

Pale yellow crystals; yield: 45 %; m.p.:105 − 110℃. IR (KBr, cm^{-1}): 3440, 3039, 2882, 2737, 2230, 1628, 1485, 1266, 1147, 892, 775, 735, 710; ^{1}H NMR (300 MHz, DMSO d_6) δ: 1.04–2.58 (m, 10*H*, piperazino-H), 3.36 (s, 2H, C<u>H</u>$_2$ of furfuryl), 4.39 (s, 2H, N-C<u>H</u>$_2$-N), 5.70 (s, 2H, NH_2), 6.90–7.15 (m, 3H, Furan-H), 7.23–7.65 (m, 5H, Ar-H) ppm; ESI-MS *m/z*: 417 $[M + H]^+$. Elemental analysis: Anal. calcd. for: $C_{23}H_{24}N_6O_2$: C, 66.33; H, 5.81; N, 20.18; O, 7.68. Found: C, 66.33; H, 5.79; N, 20.14; O, 7.64.

2.4. In vitro cytotoxicity assay

In vitro cytotoxicity of the newly synthesized compounds against human breast cancer cells (MCF-7) was performed using MTT assay according to Mosmann's method [18]. The MTT assay is based on the reduction of the soluble 3-(4, 5-methyl-2-thiazolyl)-2, 5-diphenyl-2*H*-tetrazolium bromide (MTT) into a blue-purple formazan product, mainly by mitochondrial reductase activity inside the living cells. The cells were maintained in RPMI 1640 medium (Sigma-Aldrich Inc., USA) supplemented with 10 % heat-inactivated fetal bovine serum (sigma chemicals co., USA). The cells were placed in a 96-well plate at the density of 8000 cells/well and incubated at 37℃ in a 5 % CO_2 incubator. After 24 h, the cells were treated with different concentrations (0.01–100 μM) of the newly synthesized compounds. The cells were later incubated for 72 h. The cytotoxicity of the compound was measured by adding 5 mg/ml of MTT (sigma-Aldrich Inc, USA) to each well and incubated for another 3 h. The formazan crystals of purple colour were dissolved by adding 100 μl of DMSO to each well. The absorbance was measured by a spectrophotometer at 570 nm. The cell death was calculated using the formula:-

$$\text{Cell death} = 100 - [(Tab/Cab) \times 100]$$

The assay result is expressed as the concentration of a test compound which inhibits cell growth by 50 % (IC_{50}). Each experiment was performed at least 3 times [there was a good reproducibility between replicate wells with standard errors below 10 %].

2.5. Acute toxicity study and determination of LD_{50}

LD_{50} of the most active compounds **5e** and **5g** was determined as described in the literature [19]. In this experiment, six groups of albino mice weighing between 20 g and 25 g were used. one group serves as a control and the other groups of mice were orally administrated the test compounds by gastric intubation in gradually increasing doses (100, 200, 300, 400, 500 mg/kg b. w) After 48 h of administration, the number of dead animals in each group the mean of dead animals in two successive doses (z) and the constant factor between two successive doses (d) was recorded and LD_{50} was calculated as follows.

$$\text{LD 50} = \text{the highest dose which kills all animals} - \sum(zd)/n.$$

Where, n; the number of animals in a group = 5.

2.6. Anticancer effect of compounds 5e and 5g

Adult Swiss albino mice (20–25 g) used in the study were obtained from M/s Ghosh enterprises, Kolkata, India. DAL-bearing stock female mice were obtained from the courtesy of Amala Cancer Research Centre, Thrissur, Kerala. To induce DAL in mice for the experimental study, 0.2 ml DAL – aliquot aspirated from stock was added to 9.8 ml saline (dilution 1; 50) and 0.2 ml of this diluted DAL was intraperitoneally administrated by syringe into each mouse. The DAL-injected mice were divided into four groups, each of 10 animals. Mice of group 1 (control group) were administered with 10 % DMSO as a vehicle in a volume equivalent to that given to treated animals. Group 2 and Group 3 were treated with compounds **5e** and **5g** respectively, dissolved in 10 % DMSO, at a dose of 5 mg/kg b. w (1/50 of LD_{50}). The compounds and vehicle were orally applied by gastric intubation between 10 and 12 AM daily for 2 successive weeks beginning from the 1st day of DAL injection. The median survival time

(MST) of each group containing 10 mice was noted [20]. The antitumor efficacy of compounds **5e** and **5g** was compared with that of 5FU (20 mg/kg/day i.p). MST was noted with reference to the control. Survival times of the treated groups T were compared with those of the control groups C using the following formula:-

$$\text{Increase of life span} = (\text{MST of treated group}/\text{MST of control group}) - 1 \times 100$$

2.7. Effect of compounds 5e and 5g on hematological parameter

In order to detect the influence of compounds **5e** and **5g** on the hematological status of DAL-bearing mice, Blood was obtained from the tail vein of all groups of animals, blood was drawn into RBC and WBC pipettes, diluted with dilution fluid, and counted in a Neubauer counting chamber. Hemoglobin concentration was determined by Sahli's Hemoglobinometer. A differential count was done on a freshly drawn blood film using Leishman's stain.

2.8. Statistical analysis

All the values are expressed in mean ± SEM. The data were statistically analyzed using one-way analysis of ANOVA followed by Dunnett's multiple comparison test using GraphPad InStat Software (San Diego, U.S.A) and student's *t*-test. The difference in means was considered to be significant when $P < 0.01$.

2.9. Molecular modeling studies

2.9.1. Molecular docking simulations

Molecular docking simulations were accomplished using the Glide software implemented in Schrodinger Suite (Schrödinger, Inc., USA) running on an Intel CORE i7-based HP Z230 workstation with Microsoft Windows 10 OS. The X-ray crystal structure of the protein was kept rigid, while ligands were flexible throughout the simulations.

2.9.2. Protein preparation

The X-ray solved crystal structure of the Hsp90 protein co-crystalized with a thienopyrimidine inhibitor (code: ZZ6) was retrieved from the Protein Data Bank (PDB) bearing PDB ID 2WI6 [21]. The protein was prepared under the 'Protein Preparation Wizard' of Glide employing the Optimized Potentials for Liquid Simulations 3e (OPLS3e) forcefield [22]. During the pre-processing stage, water molecules were removed, and hydrogen atoms were added. The tool also included any of the missing amino acids through the Prime module of Glide, neutralized the side chains that are not close to the binding cavity and do not participate in the formation of salt bridges. The pre-processed protein structure was refined initially by optimizing the sample-water orientation followed by a restrained minimization of the co-crystallized complex using OPLS3e, which reorients side chain hydroxyl groups and alleviates potential steric clashes. Thus, the complex obtained was minimized until it reached the convergent of a heavy atom RMSD to 0.3 Å.

2.9.3. Grid file generation

The receptor-grid generation protocol was used for defining the suitable binding site of the prepared protein for the docking process. The grid box was specified around the centroid of the cognate ligand (ZZ6) with a size of 20 Å for the docking simulations.

2.9.4. Ligand preparation

Structures of the synthesized ligands **5a-g** and ZZ6 were sketched using a 2D built panel of Maestro. LigPrep is a utility of the Schrodinger software suite that combines tools for generating 3D structures from 1D (Smiles) and 2D (SDF) representations, searching for tautomers, steric isomers and performing a geometry minimization of the ligands [22]. By employing the Ligprep protocol, all the ligands were prepared using OPLS3e with default settings.

2.9.5. Docking simulation

For the precision and accuracy of the docking protocols, the co-crystallized ligand (ZZ6) was extracted from the PDB and redocked using the Glide-docking algorithm in its extra precision (XP) mode without employing any specific constraints. An appreciable covenant between the redocked pose and the pose of the cognate ligand structure in the PDB was achieved in terms of binding orientation and molecular interactions with crucial amino acid residues of Hsp90 protein which validated the default protocols for the molecular docking of the synthesized ligands. Thus, by specifying the synthesized ligands against the receptor grid, the molecular docking simulation was performed under Glide XP mode.

2.9.6. Binding mode analysis

The generated pose viewer files were imported to the XP visualizer module of the Maestro interface and then all the protein–ligand complexes were investigated for various types of intermolecular (hydrogen bond, halogen bond, salt bridges, π-π stacking, and π-cation) interactions and binding orientation, respectively. Further, all the significant docking parameters including the docking scores and per residue interaction data were collected, accordingly.

2.10. Drug-likeliness and ADME prediction

QikProp tool of Schrodinger was used for the computational prediction of drug-likeliness and pharmacokinetic parameters. The drug-likeliness depends majorly on Lipinski's rule of five that considers molecular weight, partition coefficient (QPlogPo/w), number of hydrogen bond donors, and number of hydrogen bond acceptors. Similarly, ADME properties such as QPlogHERG, QPlogS, QPPMDCK, QPPCaco, QPlogKhsa, and % human oral absorption were also significant for the drug-like compounds [23]. All these parameters were computed for the synthesized ligands **5a-g** using QikProp tools. Initially, all the chemical structures were sketched using a 2D built panel of the LigPrep module of Maestro and are subjected to energy minimization followed by ligand preparation through the LigPrep module.

3. Results and discussion

3.1. Chemistry

The synthetic route employed for the synthesis of novel isatin-pyrimidine hybrids is outlined in Scheme 1. The starting compound 2,4 diamino-5-furfurylpyrimidine (**1**) was synthesized as per our earlier published protocol [24]. A condensation reaction between **1** and isatin (**2**) in the presence of ethanol resulted in the formation of the intermediate compound 3-{[4-amino-5-(furan-2-ylmethyl) pyrimidin-2-ylimino}-1,3-dihydro-2*H*-indol-2-one (**3**). The poor water solubility of **3** prompted us to tether it with various heterocyclic secondary amines (**4a-g**) through a methylene bridge to afford the corresponding Mannich bases as final compounds (**5a-g**). All the synthesized compounds were characterized based on their spectral data and elemental analysis (C, H, N). IR spectrum of the titled compounds showed two sharp absorption bands at 3449 cm^{-1} and 3390 cm^{-1} corresponding to the stretching vibrations of the NH_2 group. The ^1H NMR spectrum revealed the presence of signals at δ 3.36 – 3.41 ppm attributable to furfuryl CH_2 protons and a singlet at δ 4.46–4.51 ppm due to N-CH_2-N methylene protons of piperazine or heterocyclic secondary amines. In some of the ^1H NMR results, the moisture peak and the solvent DMSO peak were appeared inadvertently at δ 3.485 ppm and δ 2.514 ppm, respectively. The predicted structures of all the compounds were further agreed with the ESI-MS and elemental analyses data. The ^1H NMR, ESI-MS images, and elemental analyses of the final compounds (**5a-g**) are provided in the supporting information.

3.2. Pharmacological evaluation

3.2.1. In vitro cytotoxicity assay

All synthesized compounds were screened for their cytotoxic activity against human breast cancer cells (MCF-7) by

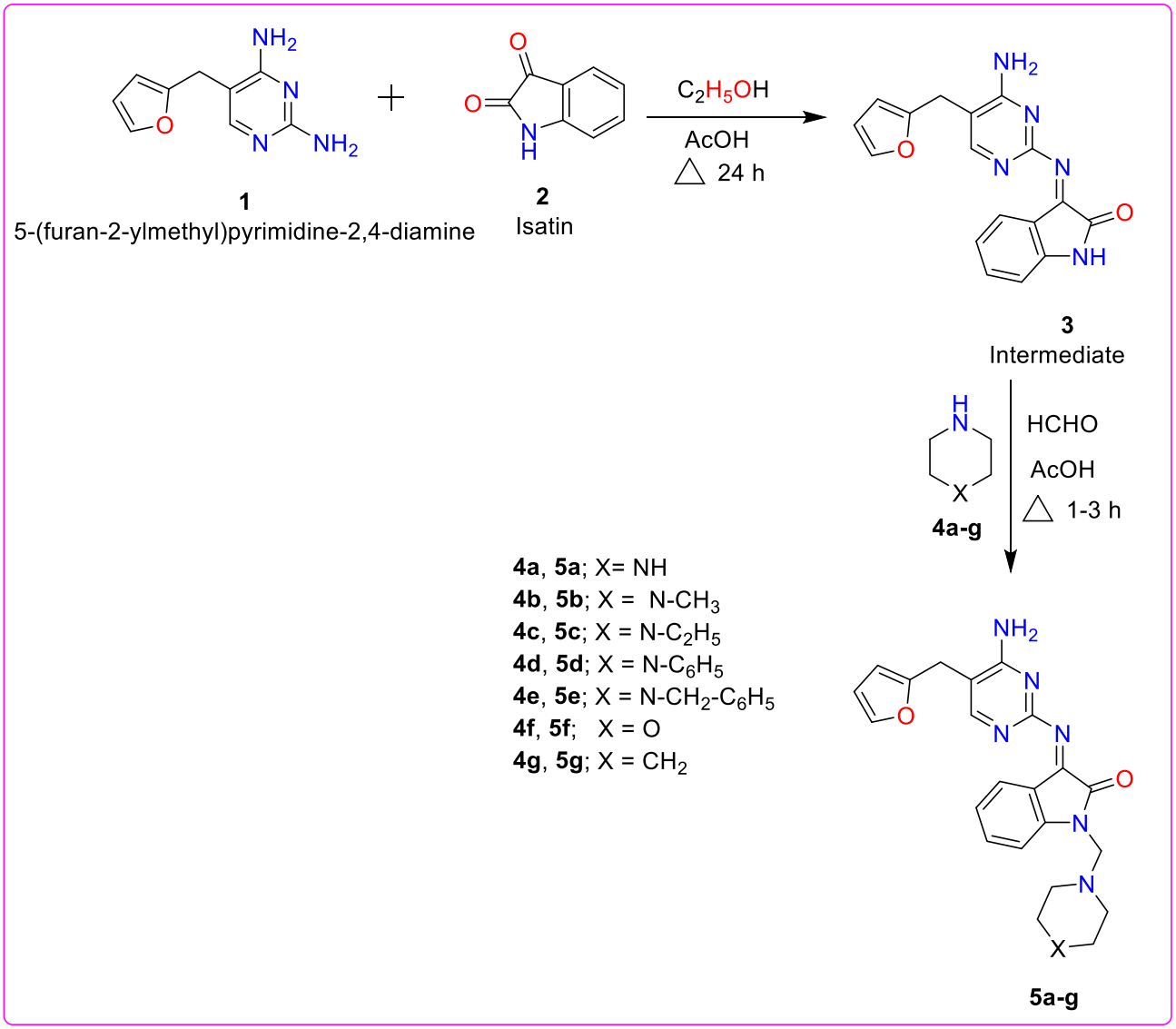

Scheme 1 Synthetic route for the synthesis of novel isatin-pyrimidine hybrid compounds **5a-g**.

in vitro MTT assay using 5-fluorouracil as a reference standard. The results for the cell growth inhibitory effects of the compounds are collected in Table 1.

All compounds displayed interesting and noteworthy cell growth inhibitory profiles with IC_{50} ranging from 12.47 to > 100 μM against the tested MCF-7 cell line (Table 1). It is evidenced from the results that the piperazine substitution on the hybrids **5a-e** showed better activity than the compounds **1**, **3**, and **5f**. Hence, it can be understood that the introduction of comparatively basic piperazine moiety directly enhances the activity, especially the compound **5e** bearing benzyl substituents at the N_4 piperazine demonstrated more potency while compared to other compounds 5b-5d bearing methyl, ethyl and phenyl substitution at the N_4-piperazine, respectively. From this structure–activity relationship (SAR) analysis, the bulky substituent such as the benzyl group on the piperazine ring imparted higher activity and is essential for the potency. Furthermore, piperidine substituted compound (**5g**) retained the cytotoxic activity than the less active compounds (**1**, **3**, and **5f**). Hence, the two most active compounds **5e** and **5g** were selected for further *in vivo* studies to confirm their potential applications as anticancer agents.

3.2.2. In vivo anticancer evaluation

An *in vivo* anticancer evaluation study was carried out for the most active compounds **5e** and **5g** using murine cancer cell Dalton's ascitic lymphoma (DAL) on mice against survival time and hematological parameters. For the determination of lethal dose $(LD)_{50}$ of **5e** and **5g**, single gradual increasing doses were orally administrated to various groups of normal albino mice. After 48 h, the number of dead animals in each group was determined and LD_{50} was calculated, LD_{50} of **5e** and **5g** was found to be 250 mg/kg b.w (Table 2).

Based on the toxicity study, the therapeutic dose for subsequent *in vivo* study was chosen to be 5 mg/kg b.w (1/50 of LD_{50}) which is so far from LD_{50}. DAL cancer cell line was introduced in either sex mice by transplantation of DAL-cells into the peritoneal cavity. The reliable criteria for judging the value of any anticancer drug are prolongation of life span, lower WBC, and higher hemoglobin levels. In the present study, the effect of the compounds **5e** and **5g** against survival time (Table 3) and capability to normalize blood picture in terms of Hemoglobin count (%), RBC count, WBC count, and the Differential count was examined. Table 4 presents the effect of compounds **5e** and **5g** on hematological parameters.

The obtained results in the Tables 3 and 4 indicated that the most active compound **5e** profoundly improved the percentage of increased life span (%ILS) to reach 91 % which is more significant ($p < 0.001$) when compared to the DAL control. Further, **5e** could significantly ($p < 0.001$) increase the percentage of haemoglobin and RBC counts. Moreover, it significantly ($p < 0.001$) decreases WBC and neutrophil counts. Thus, the best active compound **5e** decreased the mortality and improved the survival rate of DAL-bearing mice. To gain more insight into the binding mode of the highly active compound **5e**, an *in silico* molecular docking study was conducted against the structure of the Hsp90 protein.

Table 1 In vitro cytotoxicity evaluation results of the synthesized compounds.

Compounds	[a]IC_{50} (MCF-7)
1	≥100
3	≥100
5a	46.67
5b	33.87
5c	38.24
5d	40.27
5e	12.47
5f	≥100
5g	30.00
5-Fluorouracil	05.20

[a] IC_{50}: compound concentration required to inhibit tumor cell proliferation by 50%.

3.3. Molecular modeling studies

3.3.1. Molecular docking

The molecular docking approach remains one of the valuable methods to determine the possible binding mode of the ligands against any of the validated therapeutic proteins and successfully employed in research [25]. Molecular docking was conducted using the X-ray crystal structure of Hsp90 protein [Protein Data Bank (PDB) ID: 2WI6] co-crystalized with a thienopyrimidine inhibitor (code: ZZ6) [21]. Literature reports suggested that the Hsp90 protein is one of the widely distributed molecular chaperones and is majorly associated with the stability and function of several other client proteins. Moreover, Hsp90 proteins are activated in tumor cells and facilitate malignant progression which demonstrated the crucial involvement of the chaperone activity of HSP90 in cancer progression [26]. Over-expression of Hsp90 in breast cancer cells is responsible for the development of resistance to chemotherapy [27]. Hence, the crystal structure of Hsp90 was selected as a target protein for molecular docking. Prior to the docking of the synthesized ligands, the docking protocol was validated by redocking the cognate ligand (ZZ6) into the pre-defined binding site of the protein by employing the Glide XP (extra precision) module of the Schrodinger suite with default settings [28,29]. The redocked pose of ZZ6 demonstrated the same pattern of molecular interactions and binding orientation as that of the cognate ligand in PDB (ID: 2WI6). In the redocked pose of ZZ6, a strong H-bonding (1.96 Å) interaction was observed between the amide (–NH-) group of the ligand and the oxygen (O═C) of Gly97. Similarly, another strong H-bonding interaction was shown by the free amino group ($–NH_2$) with oxygen (-O═C) of the carboxylate group of Asp93 at a distance of 2.04 Å. Dichloro substituted phenyl ring exhibited hydrophobic interactions with the residues of Leu107, Phe138, and Tyr139, whereas the core thienopyrimidine moiety was surrounded by the crucial amino acids such as Asn51, Ser52, and Thr184 (Fig. 2). All these crucial interactions observed for the redocked pose of ZZ6 ligand were the same as that of the reported interactions shown by the cognate ligand in the PDB reported crystal structure. Thus, the protocol was validated for further docking of the synthesized ligand.

Based on the *in vivo* inhibition results, the most active compound **5e** was selected for the docking studies and its docking pose within the binding site of the Hsp90 protein was consid-

Table 2 Determination of LD_{50} of compounds **5e** and **5g** using the model of albino mice.

Dose (mg/kg b.w)	Total number of animals	Number of dead animals	z	d	∑ (zd)		
0		5	0		—	—	——
100		5	1		0.5	100	50
200		5	2		1.5	100	150
300		5	3		2.5	100	250
400		5	4		3.5	100	350
500		5	5		4.5	100	450

z = mean number of dead animals in two successive doses.
d = Constant factor between two successive doses.
n = number of animals in a group.
LD_{50} = the biggest dose which kill all animals – [∑ (zd)] / n.

Table 3 Effect of compounds **5e** and **5g** on survival time.

Treatment	Dose (mg/kg/day/i.p)	MST (days)	%ILS		
DAL bearing mice	—	18.5 ± 1.00	—		
Compound **5e**	5	35.4 ± 1.10		91*	
Compound **5g**	5	24.5 ± 0.90		32	
5FU	20		37.01 ± 0.8		100

*P < 0.001 vs Control, Values are expressed as mean ± SEM (n = 10), Days of drug treatment = 14.

Table 4 Effect of compounds **5e** and **5g** on hematological parameters.

Treatment	Hb (%)	RBC	WBC	Differential count (%)		
		(10^{12} / L)	(10^{12} / L)	M	N	L
Normal	14.50 ± 0.20	09.53 ± 0.01	05.85 ± 1.28	01.93 ± 0.01	17.96 ± 0.18	81.46 ± 0.16
Control#	08.75 ± 0.22	03.98 ± 0.02	19.23 ± 0.02	01.40 ± 0.04	80.13 ± 0.03	24.07 ± 0.01
5e	12.69 ± 0.45**	07.91 ± 0.01**	09.41 ± 0.01**	01.79 ± 0.02*	49.23 ± 0.01	58.32 ± 0.04
5g	10.12 ± 0.30	05.49 ± 0.03	12.43 ± 0.01*	01.58 ± 0.01	69.14 ± 0.01	33.14 ± 0.01
5FU	13.45 ± 0.69	08.79 ± 0.01	05.05 ± 0.00	01.80 ± 0.01	16.96 ± 0.01	69.46 ± 0.01

* P < 0.01.
**P < 0.001 vs Control, (n = 10).
= DAL bearing mice.

ered for the binding-mode analysis. The compound **5e** docked well into the binding site of the target protein and exhibited a network of bonded and non-bonded molecular interactions with the crucial amino acid residues (Fig. 3a). The free amino group (–NH_2) of **5e** exhibited a strong hydrogen bond interaction (1.91 Å) with an oxygen (-O═C) of Asn106. It is also interesting to note that the same basic amino acid residue Asn106 is involved in two different hydrogen bonding interactions with an oxygen atom (-O-) of isatin (2.04 Å) and furfuryl oxygen (2.36 Å), respectively. Further, the terminal phenyl ring of **5e** interacted with the basic residue Lys58 through a π-cation interaction. The isatin core moiety showed hydrophobic interactions with residues of Leu48, Asn51, Ser52, and Asp54. Hence, it was deduced that all the interactions displayed by **5e** within the binding site of the protein by *in silico* were found to be crucial for contributing to the better *in vitro* inhibition profile. Fig. 3b represents the molecular interactions of the most active ligand **5e** in its 2D interaction view.

To advance a more detailed understanding of the characteristic molecular interactions involved in the protein–ligand binding, a per-residue interaction analysis was accomplished between the ligands and the active-site amino acid residues (Table 5). Per-residue interaction analysis of the most active ligand **5e** demonstrated that the protein-inhibitor complex can be stabilized by a network of favorable van der Waals interactions (steric) perceived within the active-site residues wherein, the isatin-tethered-*N*-substituted piperazine part interacted closely with Met98 (-5.675 kcal/mol), Ile96 (-2.059 kcal/mol), Asp93 (-0.957 kcal/mol), Lys58 (-1.442 kcal/mol), Ala55 (-2.00 kcal/mol), Ser52 (-1.948 kcal/mol), Leu48 (-1.290 kcal/mol) residues, while the furfuryl conjugated aromatic amino moiety interacted similarly with Thr184 (-2.703 kcal/mol), Tyr139 (-0.570 kcal/mol), Phe138 (-3.400 kcal/mol), Leu107 (-2.426 kcal/mol), Asn106 (-6.812 kcal/mol), Asp102 (-2.977 kcal/mol). It is also important to note that an improved binding affinity of **5e** has been also

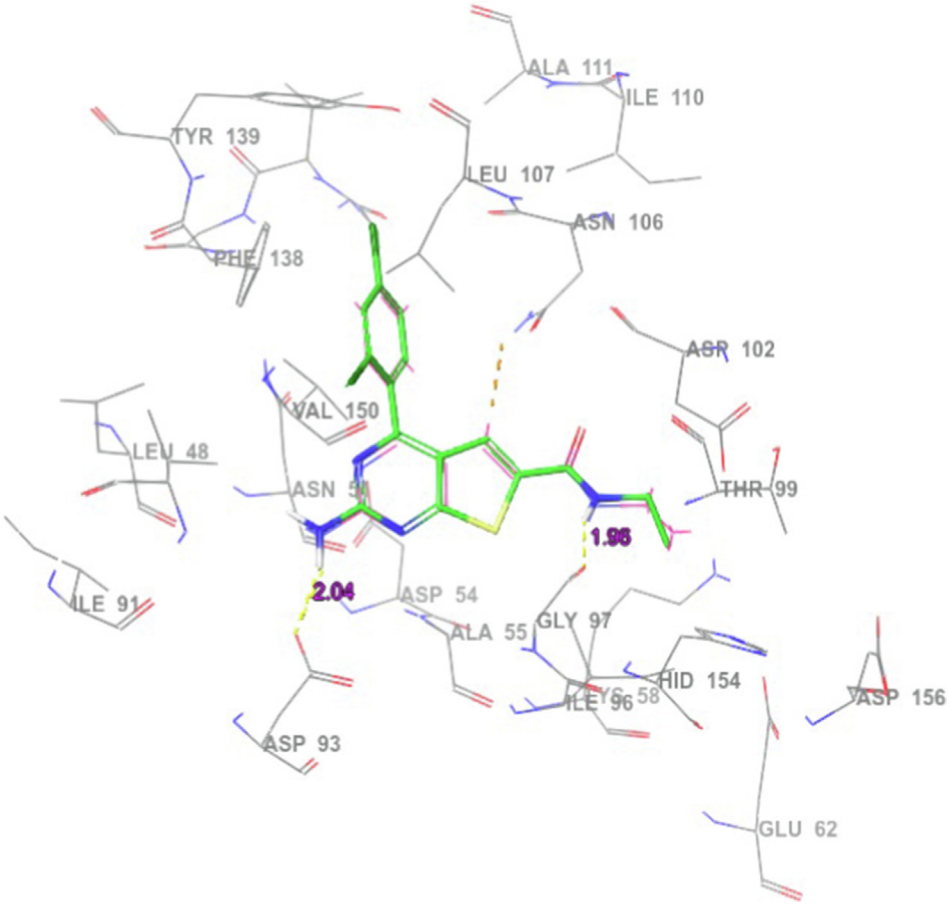

Fig. 2 The redocked pose of ZZ6 (green-coloured carbons in thick tube model) with the original pose of the co-crystallized ZZ6 extracted from the PDB (pink coloured thin tube model) in the binding site of the protein. Nonpolar hydrogen atoms were hidden for clarity and the yellow dashed line indicates hydrogen bonds.

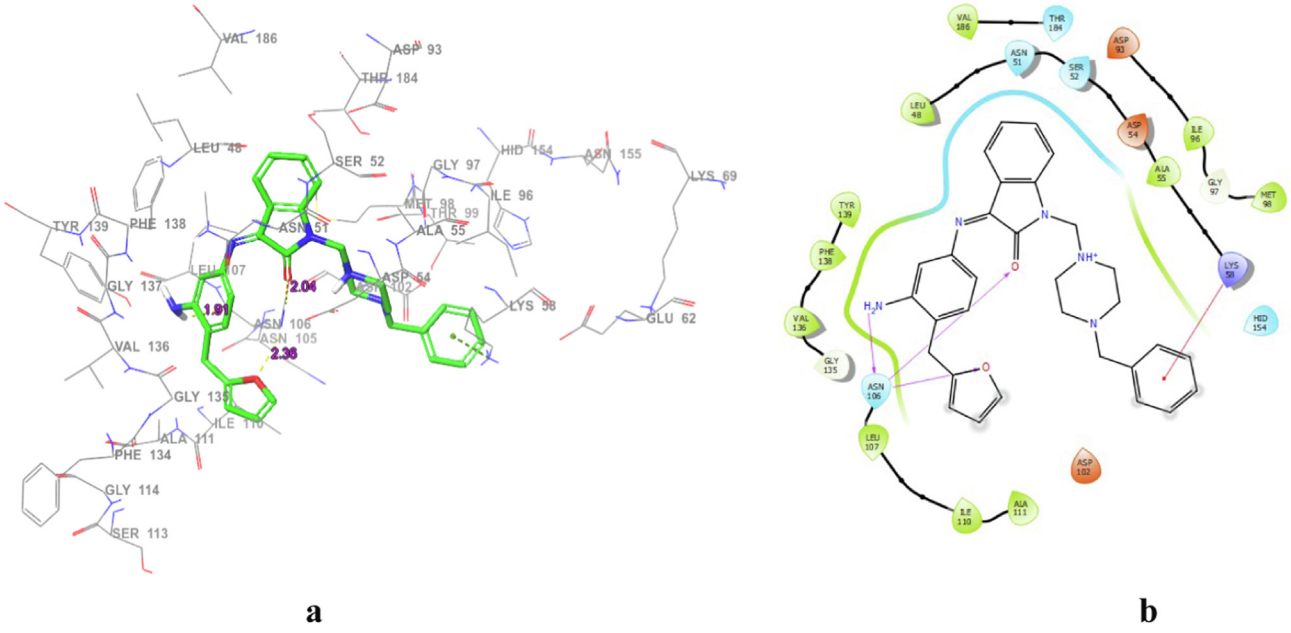

Fig. 3 Detailed molecular interactions of most active compound **5e** in 3D (**a**) and 2D (**b**) representations in alignment with the binding site residues. Non-polar hydrogen atoms were hidden for clarity and yellow dashed lines indicate hydrogen bond interactions, whereas light green coloured dashed lines designate the π-cation interaction.

Table 5 Per-residue interaction analysis data of the synthesized hybrid analogues **5a-g** within the binding-site of Hsp90.

Code	Docking score	Glide Interaction Energy (kcal/mol)	Per residue interactions		
			Van der Waals (kcal/mol)	Coulombic (kcal/mol)	H-bonding (Å)
5a	−6.73	−78.63	Thr184 (-2.362), Val150 (-0.499), Tyr139 (-1.534), Phe138 (-2.497), Leu107 (-2.807), Asn106 (-3.851), Asp102 (-3.00), Gly97 (-1.505),Ile96 (-3.386), Asp93 (-0.908), Lys58 (-2.821), Ala55 (-1.967) ,Ser52 (-1.847), Leu48 (-1.167)	Asn106 (-3.04)	Ser52 (2.05), Asn51 (2.15)
5b	−5.97	−75.80	Thr184 (-2.304), Val150 (-0.529), Tyr139 (-2.072), Leu107 (-2.926), Gly97 (-0.808), Ile96 (-2.067), Asp93 (-1.219), Lys58 (-1.646),Ala55 (-1.843), Ser52 (-1.934), Leu48 (-1.322)	Gly97 (-1.63)	Gly97 (1.91), Asn106 (1.81)
5c	−6.37	−80.17	Thr184 (-2.487), Val150 (-0.569), Tyr139 (-1.718), Phe138 (-3.237), Leu107 (-2.967), Asp102 (-2.401), Gly97 (-1.666), Ile96 (-3.281),Asp93 (-1.052), Lys58 (-2.440), Ala55 (-1.831), Ser52 (-1.941) ,Leu48 (-1.293)	Gly97 (-1.10)	Asn106 (1.80), Ser52 (2.02)
5d	−5.97	−78.51	Thr184 (-2.558), Val150 (-0.495), Tyr139 (-0.958), Phe138 (-3.615), Leu107 (-2.184), Asp102 (-2.816), Met98 (-3.752), Gly97 (-2.054),Ile96 (-3.022), Asp93 (-0.436), Lys58 (-2.489), Ala55 (-1.889) , Ser52 (-1.561), Leu48 (-1.397)	Asp93 (-2.75)	Met98 (1.92), Asn51 (2.02)
5e	−4.32	−83.44	Thr184 (-2.703), Tyr139 (-0.570), Phe138 (-3.400), Leu107 (-2.426), Asn106 (-6.812), Asp102 (-2.977), Met98 (-5.675), Ile96 (-2.059),Asp93 (-0.957), Lys58 (-1.442), Ala55 (-2.00), Ser52 (-1.948) ,Leu48 (-1.290)	Asn106 (-1.15), Gly97 (-2.00)	Asn106 (1.89), Gly97 (1.89), Ser52 (2.07)
5f	−6.36	−79.71	Thr184 (-2.370), Phe138 (-3.377), Leu107 (-2.227), Asn106 (-4.365), Asp102 (-2.95), Gly97 (-1.572), Ile96 (-3.833), Asp93 (-1.060),Lys58 (-3.219), Ala55 (-1.875), Ser52 (-1.780), Asn51 (-4.831) ,Leu48 (-0.857)	Asn106 (-3.09), Phe138 (-1.19)	Met98 (1.96), Asn51 (2.13)
5g	−5.57	−72.36	Thr184 (-2.459), Val150 (-0.502), Tyr139 (-0.942), Phe138 (-4.247), Leu107 (-2.580), Asn106 (-3.577), Asp102 (-1.969), Met98 (-4.570), Gly97 (-1.681), Ile96 (-3.422), Asp93 (-0.450), Lys58 (-3.355),Ala55 (-2.436), Asp54 (-1.139), Ser52 (-1.559), Leu48 (-1.706)	Asn106 (-3.04)	Ser52 (2.05), Asn51 (2.15)

implicated in coulombic (electrostatic) interactions observed significantly with the residues of Asn106 (-1.15 kcal/mol) and Gly97 (-2.00 kcal/mol). In general, the binding affinity data and the per-residue ligand interaction analysis recommended that a balanced network of non-bonded interactions (steric and electrostatic) complemented by hydrogen bonding contributed to the anchoring of the structure into the binding site of Hsp90. The more quantitative information gained herein can now be utilized fruitfully to conduct site-specific mutation around the nucleus to yield closer binding and potent Hsp90 protein inhibitors.

3.3.2. ADME prediction

To further characterize the drug-likeliness properties of the synthesized compounds, QikProp of Schrodinger Maestro-12.1 was employed for the determination of Lipinski's rule of five and ADME parameters by in silico [30]. The results are collected in Table 6 which indicated that the synthesized structures comply with Lipinski's rule of five. In general, the pharmacokinetic properties such as absorption, distribution, metabolism, and excretion (ADME) are very significant in the establishment of the drug candidate's safety and efficacy [31]. Human intestinal absorption (HIA) and Caco-2 permeability (QPPCaco) parameters are the indicators of intestine absorption and Caco-2 monolayer penetration. HIA data are the sum of bioavailability and absorption evaluated from the ratio of excretion or cumulative excretion in biological fluids [32]. Similarly, the QPPCaco permeability parameter describes the metabolism and drug access through the bio-membranes [33]. The predicted percentages of human oral absorption ranged from 72.1 % to 100 % in all cases and QPPCaco values ranged from 61.8 to 479.538 indicating good oral absorption of the synthesized compounds.

The partition coefficient (QPlogPo/w) and water solubility (QPlogS) are critical parameters implicated in the absorption as well as the distribution of the drugs [34]. For the synthesized compounds, QPlogPo/w and QPlogS values were calculated, which ranged from 2.241 to 4.918 and −5.946 to −2.546, respectively. Moreover, the number of violations of Jorgensen's rule of three with the recommended parameters (QPlogS > -5.7, QPPCaco > 22 nm/s, primary metabolites < 7) were also considered and the results indicated that the compounds **5c-e** deviated by one parameter out of three. Hence, QikProp predicted the physico-chemical descriptors

Table 6 The drug likeliness and in silico ADME properties of synthesized hybrid analogues **5a-g** calculated using QikProp.

Code	Drug likeliness (Lipinski's rule of five)					*In silico* ADME					
	Molecular weight	QPlogP O/W[a]	H-bond donor	H-bond acceptor	Violation of Lipinski's rule	QPlogS[b]	QPlogHERG[c]	QPPCaco[d]	QPPMDCK[e]	QPlogKhsa[f]	% human oral absorption[g]	Violation of rule of three
5a	415.494	2.241	2.5	9.0	0	−2.564	−8.007	61.8	29.875	0.107	72.1	0
5b	429.521	2.655	1.5	9.5	0	−2.763	−8.111	112.035	56.829	0.134	79.2	0
5c	443.547	3.03	1.5	9.5	0	−3.179	−8.298	105.625	53.322	0.249	80.9	1
5d	491.591	4.918	1.5	8.5	0	−5.946	−8.716	465.095	239.266	0.78	100	1
5e	505.618	4.076	1.5	9.5	1	−3.485	−8.633	125.985	64.515	0.565	75.4	1
5f	416.479	2.837	1.5	9.2	0	−3.295	−7.059	479.538	247.308	0.0	91.5	0
5g	414.506	3.805	1.5	7.5	0	−4.421	−7.313	476.245	245.472	0.435	100	0

[a] Predicted octanol/water partition co-efficient log p (acceptable range from −2.0 to 6.5).
[b] Predicted aqueous solubility in mol/L (acceptable range: −6.5 to 0.5).
[c] Predicted IC_{50} value for blockage of HERG K + channels (concern below −5.0).
[d] Predicted Caco-2 cell permeability in nm/s (acceptable range: < 25 is poor and > 500 is good).
[e] Predicted apparent MDCK cell permeability in nm/s(acceptable range: < 25 is poor and > 500 is good).
[f] Prediction of binding to human serum albumin (acceptable range: −1.5 to 1.5).
[g] Percentage of human oral absorption (< 25 % is poor and > 80 % is high).

and pharmaceutically significant properties, all of which confirmed the better drug-like properties of the synthesized compounds (Table 6 and footnote).

4. Conclusions

A simple, cost-effective, and convenient method was developed for the synthesis of novel series of isatin-pyrimidine hybrid compounds (**5a-g**) and characterized, spectroscopically. In vitro cytotoxic activities of all the final compounds **5a-g** were evaluated against human breast cancer cells (MCF-7) and identified a couple of compounds **5e** and **5g** as the most active hybrids. From the SAR study, it was observed that an increase in cytotoxic activity was achieved for the hybrids bearing piperazine moiety. Moreover, for the active compounds **5e** and **5g**, *in vivo* evaluation was carried out using murine cancer cells (DAL) on mice against survival time and hematological parameters. The remarkable results suggested that compound **5e** probably interacts with a specific protein to inhibit cell growth. Hence, the in silico molecular docking study was conducted for **5e** against Hsp90 protein and obtained crucial molecular interactions. In silico computation of the drug-likeliness and ADME properties demonstrated that the synthesized compounds had promising drug-like properties. Currently, the lead optimization and syntheses of further novel compounds with different substitutions are in progress. We trust the research findings presented here could contribute effectively to the discovery of potential novel anticancer agents.

Declaration of Competing Interest

The authors declare that they have no known competing financial interests or personal relationships that could have appeared to influence the work reported in this paper.

Acknowledgements

The authors extend their appreciation to the Deanship of Scientific Research at King Khalid University for funding this work through the Small Group Research Program (Research Grant Project number R.G.P.1/211/41). The authors are grateful to the authorities of Jadavpur University for providing the necessary facilities to carry out this research. Authors (BC and MFB) wish to thank the Management of Philadelphia University, Jordan and Centre for High Performance Computing (CHPC), Cape Town, South Africa for the support and computational resources, respectively.

Appendix A. Supplementary material

Supplementary data to this article can be found online at https://doi.org/10.1016/j.jscs.2023.101598.

References

[1] H. Sung, J. Ferlay, R.L. Siegel, M. Laversanne, I. Soerjomataram, A. Jemal, F. Bray, Global Cancer Statistics: GLOBOCAN estimates of incidence and mortality worldwide for 36 cancers in 185 Countries, CA Cancer J. Clin. 71 (2021) (2020) 209–249, https://doi.org/10.3322/caac.21660.

[2] V. Schirrmacher, From chemotherapy to biological therapy: A review of novel concepts to reduce the side effects of systemic cancer treatment (review), Int. J. Oncol. 54 (2019) 407–419, https://doi.org/10.3892/ijo.2018.4661.
[3] M.C. Pirrung, S.V. Pansare, K. Das Sarma, K.A. Keith, E.R. Kern, Combinatorial optimization of isatin-β-thiosemicarbazones as anti-poxvirus agents, J. Med. Chem. 48 (2005) 3045–3050, https://doi.org/10.1021/jm049147h.
[4] A.H. Abadi, S.M. Abou-Seri, D.E. Abdel-Rahman, C. Klein, O. Lozach, L. Meijer, Synthesis of 3-substituted-2-oxoindole analogues and their evaluation as kinase inhibitors, anticancer and antiangiogenic agents, Eur. J. Med. Chem. 41 (2006) 296–305, https://doi.org/10.1016/j.ejmech.2005.12.004.
[5] K. Kumar, S. Sagar, L. Esau, M. Kaur, V. Kumar, Synthesis of novel 1H–1,2,3-triazole tethered C-5 substituted uracil–isatin conjugates and their cytotoxic evaluation, Eur. J. Med. Chem. 58 (2012) 153–159, https://doi.org/10.1016/j.ejmech.2012.10.008.
[6] Nisha, J. Gut, P.J. Rosenthal, V. Kumar, β-amino-alcohol tethered 4-aminoquinoline-isatin conjugates: Synthesis and antimalarial evaluation, Eur. J. Med. Chem. 84 (2014) 566–573. https://doi.org/https://doi.org/10.1016/j.ejmech.2014.07.064
[7] Z.H. Chohan, H. Pervez, A. Rauf, K.M. Khan, C.T. Supuran, Isatin-derived antibacterial and antifungal compounds and their transition metal complexes, J. Enzyme Inhib. Med. Chem. 19 (2004) 417–423, https://doi.org/10.1080/14756360410001710383.
[8] V.N. Madia, A. Nicolai, A. Messore, A. De Leo, D. Ialongo, V. Tudino, F. Saccoliti, D. De Vita, L. Scipione, M. Artico, S. Taurone, L. Taglieri, R. Di Santo, S. Scarpa, R. Costi, Design, synthesis and biological evaluation of new pyrimidine derivatives as anticancer agents, Molecules 26 (2021) 771, https://doi.org/10.3390/molecules26030771.
[9] M.M. Mohamed, A.K. Khalil, E.M. Abbass, A.M. El-Naggar, Design, synthesis of new pyrimidine derivatives as anticancer and antimicrobial agents, Synth. Commun. 47 (2017) 1441–1457, https://doi.org/10.1080/00397911.2017.1332223.
[10] A. Rosowsky, R.A. Forsch, C.H. Sibley, C.B. Inderlied, S.F. Queener, New 2,4-diamino-5-(2',5'-substituted benzyl) pyrimidines as potential drugs against opportunistic infections of AIDS and other immune disorders. synthesis and species-dependent antifolate activity, J. Med. Chem. 47 (2004) 1475–1486, https://doi.org/10.1021/jm030438k.
[11] M.S. Shaikh, B. Chandrasekaran, M.B. Palkar, A.M. Kanhed, A. Kajee, K.P. Mlisana, P. Singh, M. Ghai, M. Cleopus Mahlalela, R. Karpoormath, Synthesis and biological evaluation of novel carbazole hybrids as promising antimicrobial agents, Chem. Biodivers. 17 (2020) e1900550, https://doi.org/10.1002/cbdv.201900550.
[12] B. Chandrasekaran, S. Cherukupalli, S. Karunanidhi, A. Kajee, R.R. Aleti, N. Sayyad, B. Kushwaha, S.R. Merugu, K.P. Mlisana, R. Karpoormath, Design and synthesis of novel heterofused pyrimidine analogues as effective antimicrobial agents, J. Mol. Struct. 1183 (2019) 246–255, https://doi.org/10.1016/j.molstruc.2019.01.105.
[13] M. Ajitha, K. Rajnarayana, Synthesis and evaluation of new 3-substituted-[3,4-dihydro pyrimidinones]-indolin-2-ones for anti inflammatory activity, Int. J. Pharma Bio Sci. 2 (2011) 81–90.
[14] S. Karunanidhi, B. Chandrasekaran, R. Karpoormath, H.M. Patel, F.B. Kayamba, S. Reddy Merugu, V. Kumar, S. Dhawan, B. Kushwaha, M. Cleopus Mahlalela, Novel thiomorpholine tethered isatin hydrazones as potential inhibitors of resistant mycobacterium tuberculosis, Bioorg. Chem. (2021), https://doi.org/10.1016/j.bioorg.2021.105133 105133.
[15] R. Kumar, M. Kumar, Synthesis of novel 5-Bromoisatin based pyrimidine derivatives and their antimicrobial evaluation, Asian J. Pharm. Pharmacol. 5 (2019) 1244–1250, https://doi.org/10.31024/ajpp.2019.5.6.24.
[16] K. Meenakshi, G. Natesan, M. Sarangapani, Synthesis, characterization and antimicrobial activity of some novel schiff and mannich bases of Isatin, Int. J. Pharm. Pharm. Sci. 6 (2014) 318–322.
[17] P. Selvam, N. Murgesh, M. Chandramohan, E. De Clercq, E. Keyaerts, L. Vijgen, P. Maes, J. Neyts, M.V. Ranst, In vitro antiviral activity of some novel isatin derivatives against HCV and SARS-CoV viruses, Indian J. Pharm. Sci. 70 (2008) 91–94, https://doi.org/10.4103/0250-474X.40339.
[18] T. Mosmann, Rapid colorimetric assay for cellular growth and survival: application to proliferation and cytotoxicity assays, J. Immunol. Methods 65 (1983) 55–63, https://doi.org/10.1016/0022-1759(83)90303-4.
[19] N.A. Afifi, A. Ramadan, E.A. El-Kashoury, H.A. El-Banna, Some pharmacological activities of essential oils of certain umbelliferous fruits, Vet. Med. J. Giza 42 (1994) 85–92.
[20] M.I. Sriram, S.B.M. Kanth, K. Kalishwaralal, S. Gurunathan, Antitumor activity of silver nanoparticles in Dalton's lymphoma ascites tumor model, Int. J. Nanomed. 5 (2010) 753–762, https://doi.org/10.2147/IJN.S11727.
[21] P.A. Brough, X. Barril, J. Borgognoni, P. Chene, N.G.M. Davies, B. Davis, M.J. Drysdale, B. Dymock, S.A. Eccles, C. Garcia-Echeverria, C. Fromont, A. Hayes, R.E. Hubbard, A.M. Jordan, M.R. Jensen, A. Massey, A. Merrett, A. Padfield, R. Parsons, T. Radimerski, F.I. Raynaud, A. Robertson, S.D. Roughley, J. Schoepfer, H. Simmonite, S.Y. Sharp, A. Surgenor, M. Valenti, S. Walls, P. Webb, M. Wood, P. Workman, L. Wright, Combining hit identification strategies: fragment-based and in silico approaches to orally active 2-Aminothieno[2,3-d] pyrimidine inhibitors of the Hsp90 molecular chaperone, J. Med. Chem. 52 (2009) 4794–4809, https://doi.org/10.1021/jm900357y.
[22] S.F. Giardina, D.S. Werner, M. Pingle, P.B. Feinberg, K.W. Foreman, D.E. Bergstrom, L.D. Arnold, F. Barany, Novel, self-assembling dimeric inhibitors of human β Tryptase, J. Med. Chem. 63 (2020) 3004–3027, https://doi.org/10.1021/acs.jmedchem.9b01689.
[23] F. Ntie-Kang, An in silico evaluation of the ADMET profile of the StreptomeDB database, Springerplus 2 (2013) 353, https://doi.org/10.1186/2193-1801-2-353.
[24] R. Rajapandi, J. Singh, T.K. Maity, Improved synthesis of novel 2,4-diamino-5-furfurylpyrimidine in presence of molecular sieves, Asian J. Chem. 22 (2010) 1841–1844.
[25] V. Salmaso, S. Moro, Bridging molecular docking to molecular dynamics in exploring ligand-protein recognition process: an overview, Front. Pharmacol. 9 (2018) 923, https://doi.org/10.3389/fphar.2018.00923.
[26] D. Mahalingam, R. Swords, J.S. Carew, S.T. Nawrocki, K. Bhalla, F.J. Giles, Targeting HSP90 for cancer therapy, Br. J. Cancer 100 (2009) 1523–1529, https://doi.org/10.1038/sj.bjc.6605066.
[27] S. Tsutsumi, L. Neckers, Extracellular heat shock protein 90: a role for a molecular chaperone in cell motility and cancer metastasis, Cancer Sci. 98 (2007) 1536–1539, https://doi.org/10.1111/j.1349-7006.2007.00561.x.
[28] R.A. Friesner, J.L. Banks, R.B. Murphy, T.A. Halgren, J.J. Klicic, D.T. Mainz, M.P. Repasky, E.H. Knoll, M. Shelley, J.K. Perry, D.E. Shaw, P. Francis, P.S. Shenkin, Glide: a new approach for rapid, accurate docking and scoring. 1. method and assessment of docking accuracy, J. Med. Chem. 47 (2004) 1739–1749, https://doi.org/10.1021/jm0306430.
[29] S. Cherukupalli, B. Chandrasekaran, R.R. Aleti, N. Sayyad, G. A. Hampannavar, S.R. Merugu, H.R. Rachamalla, R. Banerjee, R. Karpoormath, Synthesis of 4,6-disubstituted pyrazolo[3,4-d] pyrimidine analogues: cyclin-dependent kinase 2 (CDK2) inhibition, molecular docking and anticancer evaluation, J. Mol. Struct. 1176 (2019) 538–551, https://doi.org/10.1016/j.molstruc.2018.08.104.

[30] A. Dagan-Wiener, I. Nissim, N. Ben Abu, G. Borgonovo, A. Bassoli, M.Y. Niv, Bitter or not? BitterPredict, a tool for predicting taste from chemical structure, Sci. Rep. 7 (2017) 12074, https://doi.org/10.1038/s41598-017-12359-7.

[31] A.J. Lucas, J.L. Sproston, P. Barton, R.J. Riley, Estimating human ADME properties, pharmacokinetic parameters and likely clinical dose in drug discovery, Expert Opin. Drug Discov. 14 (2019) 1313–1327, https://doi.org/10.1080/17460441.2019.1660642.

[32] Y.H. Zhao, J. Le, M.H. Abraham, A. Hersey, P.J. Eddershaw, C.N. Luscombe, D. Boutina, G. Beck, B. Sherborne, I. Cooper, J.A. Platts, Evaluation of human intestinal absorption data and subsequent derivation of a quantitative structure - activity relationship (QSAR) with the Abraham descriptors, J. Pharm. Sci. 90 (2001) 749–784, https://doi.org/10.1002/jps.1031.

[33] Y. Kamiya, H. Takaku, R. Yamada, C. Akase, Y. Abe, Y. Sekiguchi, N. Murayama, M. Shimizu, M. Kitajima, F. Shono, K. Funatsu, H. Yamazaki, Determination and prediction of permeability across intestinal epithelial cell monolayer of a diverse range of industrial chemicals/drugs for estimation of oral absorption as a putative marker of hepatotoxicity, Toxicol. Reports 7 (2020) 149–154, https://doi.org/10.1016/j.toxrep.2020.01.004.

[34] W. Jorgensen, E. Duffy, Prediction of drug solubility from structure, Adv. Drug Deliv. Rev. 54 (2002) 355–366, https://doi.org/10.1016/S0169-409X(02)00008-X.